


RESEARCH ARTICLE

# Optimization and synthesis on the dynamics performance of the tensioning and relaxing wearable system in a novel knee exoskeleton using co-simulation

Yuwei Yang<sup>1,2</sup>, Jiapeng Yin<sup>1,2</sup> , Wenyao Qi<sup>1,2</sup>, Zhaotong Li<sup>1,2</sup>, Zuyi Zhou<sup>1,2</sup>, Zhongyu Liu<sup>3</sup> and Jinyou Xu<sup>1,2</sup>

<sup>1</sup>Tianjin Key Laboratory for Advanced Mechatronic System Design and Intelligent Control, School of Mechanical Engineering, Tianjin University of Technology, Tianjin 300384, China

<sup>2</sup>National Demonstration Center for Experimental Mechanical and Electrical Engineering Education, Tianjin University of Technology, Tianjin 300384, China

<sup>3</sup>Department of Traumatic Orthopaedics, Tianjin Hospital, Tianjin 300211, China

**Corresponding author:** Jinyou Xu; Email: [xujinyou@126.com](mailto:xujinyou@126.com)

**Received:** 25 April 2024; **Revised:** 22 August 2024; **Accepted:** 18 September 2024; **First published online:** 31 October 2024

**Keywords:** knee joint exoskeleton robot; wearing comfort; human-machine parallel; co-simulation; overrunning clutch

## Abstract

In this paper, a novel tensioning and relaxing wearable system is introduced to improve the wearing comfort and load-bearing capabilities of knee exoskeletons. The research prototype of the novel system, which features a distinctive overrunning clutch drive, is presented. Through co-simulation with ANSYS, MATLAB, and SOLIDWORKS software, a comprehensive multi-objective optimization is performed to enhance the dynamics performance of the prototype. Firstly, the wearing contact stiffness of the prototype and the mechanical parameters of the relevant materials are simulated and fitted based on the principle of functional equivalence. And then, its equivalent nonlinear circumferential stiffness model is obtained. Secondly, to enhance the wearing comfort of the exoskeleton, a novel comprehensive performance evaluation index, termed wearing comfort, is introduced. The index considers multiple factors such as the duration of vibration transition, the acceleration encountered during wear, and the average pressure applied. Finally, through the utilization of this indicator, the system's dynamics performance is optimized via multi-platform co-simulation, and the simulation results validate the effectiveness of the research method and the proposed wearable comfort index. The theoretical basis for the subsequent research on the effectiveness of prototype weight-bearing is provided.

## 1. Introduction

In recent years, the prominence of aging in society has led to a rise in chronic knee diseases, with knee osteoarthritis (KOA) emerging as the most prevalent [1, 2]. Treatment options typically include surgery, medication, and assistive devices. However, surgery entails substantial costs and prolonged recovery periods, while pharmaceutical treatments may necessitate time to manifest efficacy [3]. Utilizing exoskeletons to reduce the axial impact load on knee joint soft tissues holds significant implications for the prevention and rehabilitation of KOA. [4]. Existing research on exoskeleton robots primarily emphasizes structural design, with limited investigation into the wearability performance influenced by factors such as gait cycle alterations during human-machine interaction. For instance, Wang, J. et al. [5] proposed a lower limb exoskeleton based on the biomechanics of the knee joint to accommodate knee movement, while optimizing the positioning and layout of the wearable device to reduce undesired interaction forces between the user and the machine. Long, Y. et al. [6] introduced a highly portable and compact active knee exoskeleton for patients with knee joint impairments, consisting only of the knee

joint section and a driving control module. Placing the driving control module at the waist reduces the weight of the lower limb exoskeleton, allowing it to weigh only 1.3 kg when worn on one leg. Ostrach, B. et al. [7] introduced an unpowered knee exoskeleton robot that utilizes a spring mechanism at the knee joint to convert elastic potential energy into kinetic energy during knee flexion, thereby making walking, running, and jumping more energy-efficient for the wearer. Li, H. [8] designed various adaptive/passive compensation mechanisms for the exoskeleton at the wearable position to improve comfort. Zimmermann, Y. [9] developed an exoskeleton human-machine attachment system that ensures alignment of the limb positioning axis for comfort through the controlled extension and retraction of cables.

The aforementioned lower limb knee exoskeleton reduces undesired human-robot interaction forces by optimizing strap placement and minimizing exoskeleton weight. While these measures indeed enhance comfort to a certain extent, issues persist regarding restricted blood circulation in local tissues due to the fixed binding method. This particularly hinders long-term wearing and usage of exoskeleton robots, especially for rehabilitation and prevention purposes. Therefore, in order to address the biomechanical characteristics of lower limb movement during the gait cycle [10], an exoskeleton system should possess a high wearing contact stiffness during the “stance phase” to effectively support and distribute the body’s movement loads, thereby reducing pressure on joints and bones and enhancing walking stability. Conversely, during the “swing phase,” a lower wearing contact stiffness is required to promote local blood circulation and ensure unimpeded blood supply [11, 12]. Through the integration of the human-machine coupling dynamic properties of lower limb rehabilitation training [13], exoskeleton systems provide wearers with optimal support and comfort during different walking phases, thereby enabling enhanced assistance and rehabilitation effects.

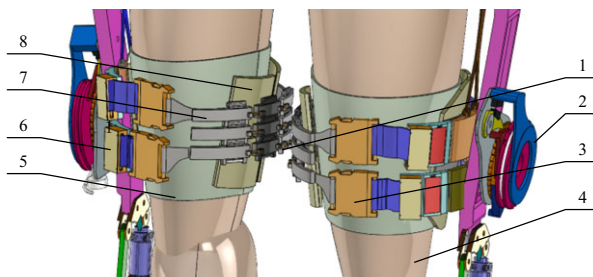
To effectively introduce and implement biomimetic working mechanisms, it is essential to consider the dynamic and static distribution of contact stress between exoskeleton devices and the human body [14]. According to Fineberg, D. B. et al. [15], the use of traditional exoskeletons may induce discomfort due to the high shear and friction forces they exert on the skin. Jose L, P. [16] and Krouskop, T. A. et al. [17] suggest that establishing the precise mathematical correlation between human-machine contact pressure and comfort during wear poses challenges. The utilization of biological skin pressure sensors in testing can only partially capture the association between pressure and comfort. Luan, Y. et al. [18] recommend that the compressive stress on muscle tissue should not exceed 56 kPa to ensure comfort while wearing exoskeleton devices. The exoskeleton wearable system in this type of research is a complex nonlinear system that involves many factors. A single mathematical model is difficult to accurately describe the overall dynamic characteristics during movement. [19] Therefore, co-simulation of the exoskeleton system using ANSYS, MATLAB, and SOLIDWORKS platforms can be utilized to analyze the performance indicators of the exoskeleton system in a more realistic manner. [20, 21].

This paper presents a novel tensioning and relaxing wearable system incorporating an overrunning clutch drive to improve the comfort of knee joint exoskeleton robots [22]. The system, developed in conjunction with the research group’s patented inventions [23, 24] and related research, is analyzed for its biomimetic principles and underwent thorough performance optimization studies.

## 2. Explore research prototypes and their biomimetic working mechanisms

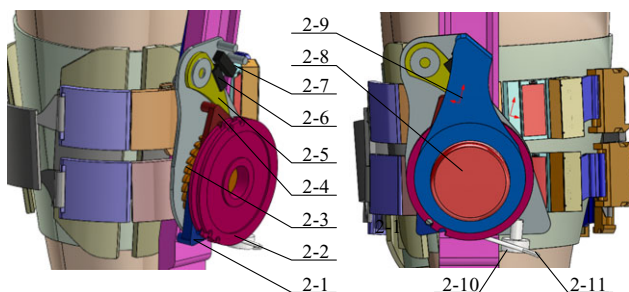
Based on the biomechanical features of the human lower limb locomotion [25], a novel prototype of the tensioning and relaxing wearable system with variable stiffness relaxation self-locking function is proposed, as illustrated in Figs. 1 and 2.

The human-machine parallel research prototype comprises two main components. The one component comprises a nonlinear contact stiffness model that integrates mechanical parameters of muscle tissue and contact parameters of the buffer layer armor. The other component consists of the motor overrunning clutch drive unit, enabling control and adjustment of the exoskeleton binding device. The overrunning clutch functions in the following manner.



1 Spring and damping 2 Overrunning clutch drive unit 3 Snap fastener 4 Muscle tissue  
5 Tight protection layer 6 Adjustment device 7 Exoskeleton articulated armor layer  
8 Exoskeleton cushioning layer

**Figure 1.** Human-machine parallel tensioning and relaxing wearable system.



2-1 Clutch lower stopper post 2-2 Pulley 2-3 Ratchet wheel 2-4 Clutch upper stopper post  
2-5 Ratchet pawl 2-6 Permanent magnet lower end 2-7 Permanent magnet upper end  
2-8 Stepping motor 2-9 Front cover 2-10 Limit wheel 2-11 Spring damped pull rope

**Figure 2.** Overrunning clutch assembly.

### 2.1. Stance phase

At the initiation of the stance phase, activate the stepper motor to drive the internal ratchet clockwise. With the ongoing rotation, the linear spring progressively extends, initiating the energy accumulation.

During the stance phase, the stepper motor remains in motion, tightening the left armor layer by engaging the linear spring and damping device. The tension is subsequently transmitted to the right armor layer. Upon reaching the designated angle and halting, the ratchet and pawl mechanism automatically secures to prevent reverse rotation, thereby maintaining the extension of the linear spring. This action increased the normal load on the body within the tension and relaxation-wearing system, thereby augmenting assistance through enhanced contact stiffness.

At the end of the stance phase, the stepper motor rotates clockwise again by a certain angle and then stops, so that the front end of the pawl is adsorbed onto the permanent magnet, relieving the self-locking of the clutch.

### 2.2. Swing phase

Upon disengagement of the self-locking mechanism at the beginning of swing phase, the spring expels its stored energy, leading to rapid retraction of the spring and damping system to the right. Simultaneously, the torsion spring begins to accumulate force as a result of the swift retraction.

During the continuous and final stages of the swing phase, the ratchet reverses with the assistance of the external torsion spring connected to the stepper motor. The elastic potential energy of the torsion spring is discharged, causing the lower gear column to transition to the upper left position of

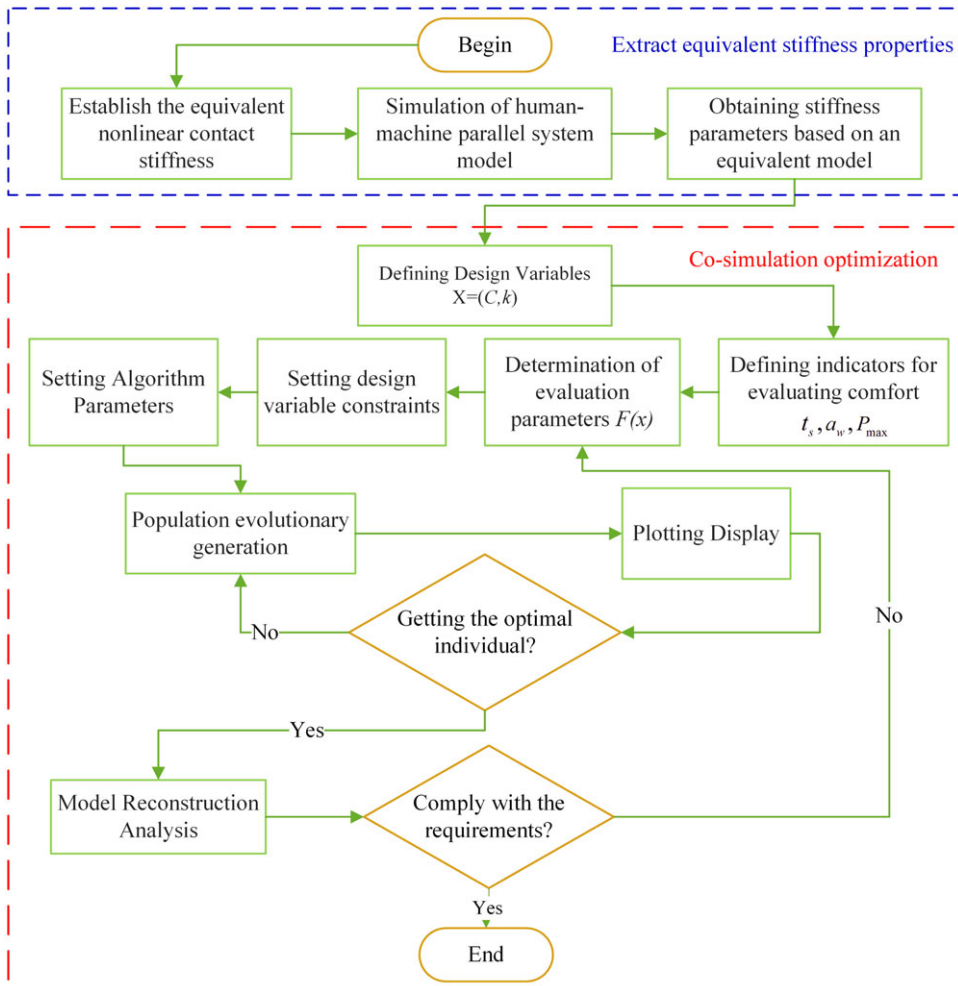


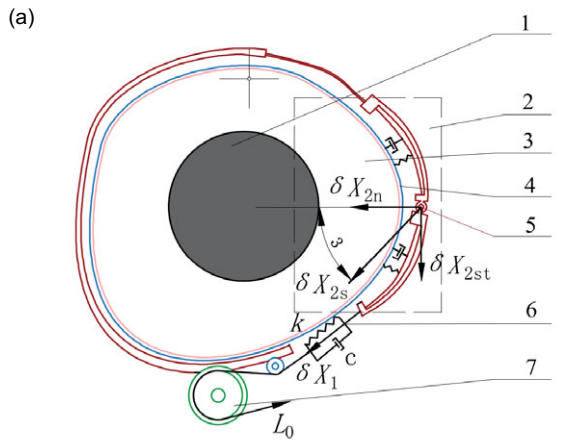
Figure 3. Optimization process.

the pawl. Subsequently, the pawl is displaced from the upper end of the permanent magnet to secure the ratchet, restricting the clutch’s rotation to clockwise movement. This sequence signifies the completion of a full cycle of clutch operation, preparing for the initiation of the subsequent supporting phase.

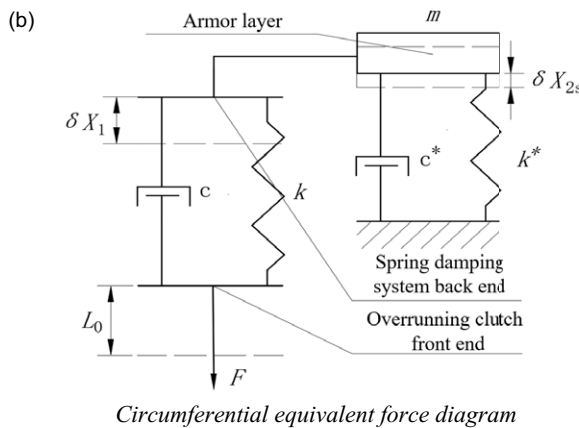
The research prototype features a biomimetic working mechanism that, when integrated with an overrunning clutch, enhances the comfort and flexibility of the exoskeleton [26]. This improvement results in increased adaptability, offering users support and assistance during exoskeleton use.

### 3. Synthesis of dynamics performance

In order to facilitate a deeper comprehension of the aforementioned bionic working mechanism, this study presents a synthesis of the system dynamics performance. This study utilizes a multi-objective genetic algorithm [27], the functional equivalence principle, and finite element simulation to thoroughly investigate the optimization of prototype dynamics performance. The optimization process is depicted in Figure 3.



1 Bone tissue-fixation support 2 Nonlinear contact stiffness mode 3 muscular tissue  
4 Braided fabric 5 Armor layer 6 Spring damping system 7 Overrunning Clutch  
Top view of wear



Circumferential equivalent force diagram

Figure 4. Schematic diagram of man-machine parallel tension wearing system.

### 3.1. Constructing equivalent nonlinear contact stiffness models

Constructing an equivalent nonlinear contact stiffness model and analyzing the load conditions based on simulation requirements can be challenging due to the complex contact relationship of the model. Hence, traditional scientific experiments cannot yield the circumferential driving trajectory of the nonlinear contact stiffness model as  $X_n$  varies. In the study of dynamics system mechanisms, the principle of equivalent substitution is a useful and efficient method.

This paper utilizes the principle of functional equivalence to address the issue at hand. Specifically, the nonlinear contact stiffness model of the dashed part in Figure 4 (a) top view is analyzed separately using virtual prototype simulation. By extracting the nonlinear stiffness in the circumferential direction of a nonlinear contact stiffness model under the swing phase, the displacement of the spring damping system over time can be precisely measured. This displacement serves as input excitation to regulate the relaxation state of the overrunning clutch [28]. Through this transformation, the equivalent excitation is replaced by the circumferential displacement in the nonlinear stiffness model in the equivalent force diagram depicted in Figure 4 (b). This approach effectively controls and optimizes the motion characteristics and safety performance of the entire system.

During the supporting phase of the gait cycle ( $0 \sim 0.72$  s), as a result of the tension effect of the clutch unit in the circumferential direction, the linear spring and damping device are progressively tightened

**Table I.** Results of overloading for 3 Experimental setups.

Component name	Boundary condition	Friction factor	Contact stiffness
Armor Layer Connections	Revolute	0	
Armor Layer – Buffer Layer	Binding contact		1
Buffer Layer – Muscle Issue	Friction contact	0.37	0.01

through the rotation of the stepper motor. This action then pulls the armor layer, leading to a tensile amount in the thigh’s circumferential direction  $\delta X_1$ . The spring is inclined at an angle of  $\varepsilon = 42^\circ$  to the central axis of the connecting pair due to the presence of limit wheels, causing deformation  $\delta X_{2s}$  in the circumferential direction of the thigh according to the nonlinear contact stiffness model. When considering the total stretching amount  $L_0$ , it is important to control the radial deformation of muscle tissue, denoted as  $X_{2n}$ , below the critical tolerance value for human surface to radial deformation during the design process [29]. Through the study of geometric relationships, it can be determined that:

$$\delta X_1 = L_0 - \delta X_{2s} \tag{1}$$

The magnitude of normal deformation in the nonlinear contact stiffness model may be represented as:

$$\delta X_{2n} = \delta X_{2s} \sin \varepsilon \tag{2}$$

In the same way, the restricted circumferential acceleration  $a_s$  can be broken down into normal acceleration  $a_n$  and tangential acceleration  $a_{st}$ . As the system transitions into a relaxed state during the swinging phase (0.72 s ~ 1.2 s), it does so because of the quick release of the spring’s elastic potential energy. The decrease in contact stiffness over a brief period in this phase may lead to minimal fluctuations in the load transferred to the human body.

### 3.2. Dynamics analysis of a prototype human-machine parallel research

#### 3.2.1. Virtual prototype based equivalent dynamics simulation

At the beginning and duration of the stance phase of the walking cycle, muscle tissue experiences significant load, resulting in nonlinear deformation. This study utilizes ANSYS finite element analysis software and follows the modeling approach outlined in reference [30]. Muscle tissue is defined using Mooney-Rivlin type hyperelastic materials. As shown in Table I, the linear displacement loads and boundary conditions of the contact surface settings and the material mechanical parameters of each part of the finite element model. A dynamics virtual prototype model of a human-machine parallel tension and relaxation wearable system is constructed, as depicted in Figure 5. This model aims to accurately simulate the circumferential stretching trajectory of the nonlinear contact stiffness model under operational conditions. The simulation results of this model are presented in Figure 6.

#### 3.2.2. Nonlinear fitting of equivalent model stiffness properties

Mooney-Rivlin type materials exhibit superelasticity and hysteresis, causing nonlinear changes in the circumferential tension of the spring damping system [31]. To reduce errors, a polynomial fitting method is used to address the issue of discontinuous changes in discrete circumferential stretching trajectory data. By adjusting the stiffness ( $K_1$ ) of the linear spring in the experiment, the hyperelastic characteristics of the model in the circumferential direction were fitted into three different sets of nonlinear composite equivalent wearing stiffness curves, as shown in Figure 7.

Based on the three nonlinear equivalent wearing stiffness curves in Figure 7, it is evident that when the linear spring stiffness exceeds 2000N/m, there is some fluctuation in the stiffness curve. Therefore, for the extraction of clutch circumferential trajectory driving data, the stiffness model  $K_1 = 2000$  N/m should be used to ensure the rationality and reliability of the data.

Considering the characteristics of the equivalent nonlinear contact stiffness model, and with the data support of the circumferential stiffness of the nonlinear contact stiffness model in Figure 7, the



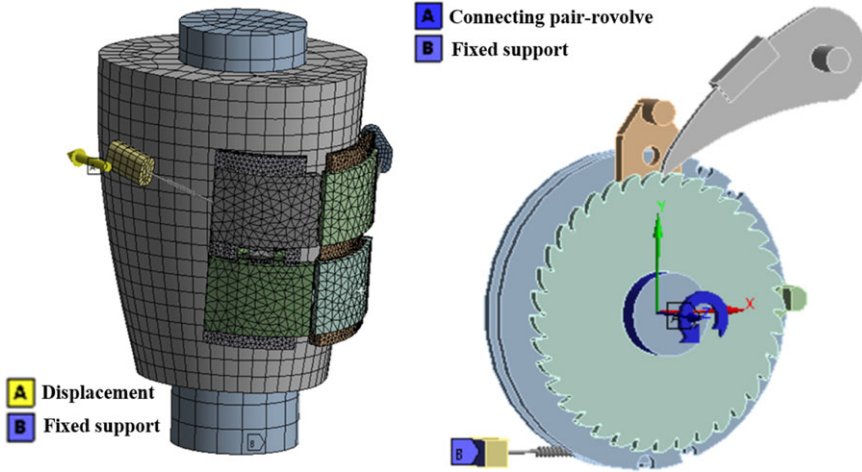


Figure 5. Boundary conditions of finite element model.

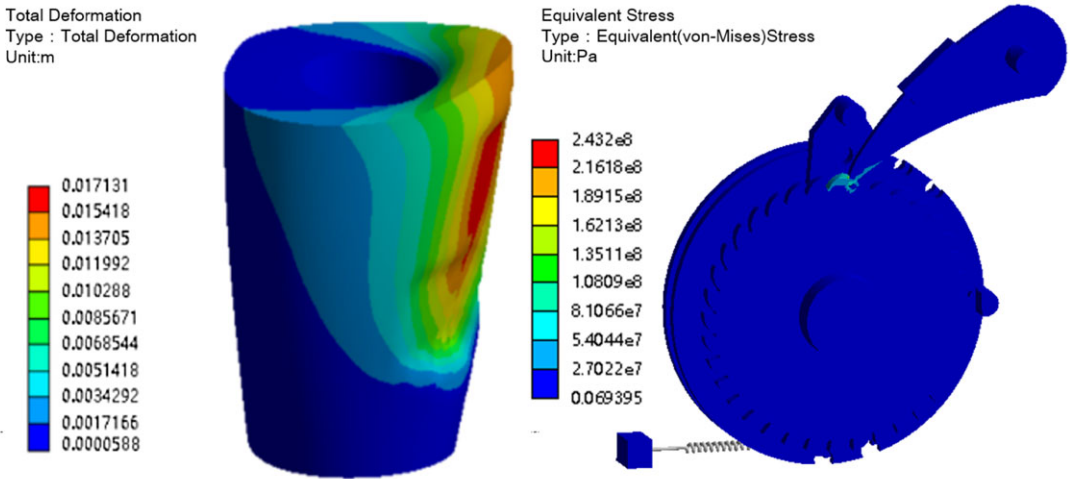


Figure 6. Finite element model analysis results.

circumferential stretch of the spring-damped system with  $K_1 = 2000 \text{ N/m}$  is used as the driving condition for the trajectory. The linear rotational load under the standard working condition (corresponding to the trajectory of the equivalent stiffness model) is applied to the clutch ratchet. The results of the dynamics analysis of the system are shown in Figure 6, and the vibration and pressure data of the human tissues in the system can be obtained by extracting the data of the spring probe in the model. The results under different vibration parameters are shown in Table II.

Two vibration parameters that affect human comfort evaluation, the elastic modulus  $x_E$  of the damper damping buffer layer and the torsional spring stiffness  $x_s$  connecting the stepper drive motor and the over-running clutch, are selected as design variables based on research data on human tolerance to vibration and compression environments [32]. Using virtual prototype simulation data of an exoskeleton wearable system under design variable, a wearing comfort evaluation function  $F(x)$  is determined.

To conduct multi-objective genetic optimization for wearability follow-up research, one must consider the dynamic characteristics of system vibration during the physical interaction between humans and machines, as well as the impact of soft tissue stress distribution on the wearability of exoskeletons

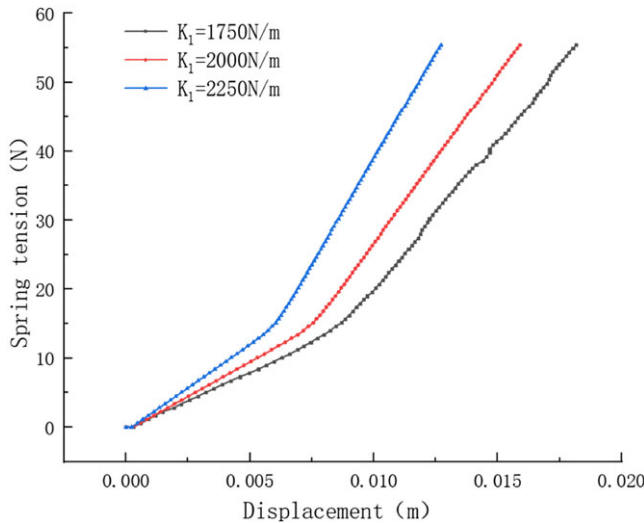


Figure 7. Nonlinear equivalent wearing stiffness model in circumferential direction.

[18]. To construct the wearability evaluation index of the rigid-flexible coupling dynamics system, a linear weighted sum method is utilized. The wearability comfort function [33] can be represented by equation:

$$F_{\min} = \min_{x \in D} \left( \sum_{i=1}^l w_i f_i(x) \right) \tag{3}$$

where  $f_i(x)$  represents the three sets of quantitative indicator evaluation functions in the comfort evaluation model, while  $l$  represents the number of quantitative indicator evaluation functions.  $w_i$  is a set of weights in the comfort objective function, and it satisfies the following equation:

$$\sum_{i=1}^l w_i = 1, w_i \geq 0 \tag{4}$$

In the optimization process, reference is made to “Mechanical Vibration and Shock – Evaluation of Human Exposure to Whole Body Vibration” [34], Table II shows that the objective of the constraint is to ensure that the vibration-weighted root mean square acceleration value does not exceed 0.315 m/s<sup>2</sup>. Additionally, it is important to include transition time  $t_s$  to thoroughly assess the comfort of wearing the exoskeleton. According to literature [18], the pressure at the wearing point of the exoskeleton should not exceed 56 kPa. Taking into account relevant literature on vibration and comfort evaluation, three quantitative evaluation functions are selected for comfort evaluation: the vibration transition time (adjustment time)  $t_s$  of the spring damping system, the weighted root mean square value of the normal acceleration  $a_w$  at the wearing point of the knee exoskeleton, and the maximum normal average pressure  $P_{\max}$  of the human-machine contact surface. The evaluation function for the system’s vibration transition time  $t_s$  can be seen in equation:

$$t_s(x) = C_1 x_c^2 + C_2 x_c + C_3 x_k^2 - C_4 x_k + C_5 \tag{5}$$

The evaluation function of the  $a_w$  at the exoskeleton-wearing site can be expressed as equation:

$$a_w(x) = C_6 x_c^2 + C_7 x_c + C_8 x_k^2 - C_9 x_k + C_{10} \tag{6}$$

The evaluation function of the  $P_{\max}$  on the human-machine contact surface can be expressed as equation:

$$P_{\max}(x) = C_{11} x_c^2 + C_{12} x_c + C_{13} x_k^2 - C_{14} x_k + C_{15} \tag{7}$$



**Table II.** The relationship between normal acceleration and intuitive perception in the human body.

Root mean square value of normal acceleration on human body	Human intuition
Less than 0.315 m/s <sup>2</sup>	Comfortable
0.315 m/s <sup>2</sup> ~ 0.65 m/s <sup>2</sup>	A little uncomfortable
0.65 m/s <sup>2</sup> ~ 1 m/s <sup>2</sup>	Uncomfortable
1 m/s <sup>2</sup> ~ 1.5 m/s <sup>2</sup>	Quite uncomfortable
More than 1.5 m/s <sup>2</sup>	Very uncomfortable

**Table III.** Multi-objective values before and after optimization.

	$C(\text{Ns/mm})$	$k(\text{Nm}^\circ)$	$t_s(\text{s})$	$a_w(\text{m/s}^2)$	$P_{\max}(\text{Pa})$
Pre-optimization	0.1	1	0.184	0.196	16,629
Post-optimization	0.302	1.098	0.056	0.159	16,767
Optimal quantity	0.202	0.098	69%	19%	-1%

Equations (5) ~ (7) represent the damping of the damper in the finite element model as  $x_c$ , the stiffness of the torsion spring connecting the stepper drive motor and the overrunning clutch as  $x_k$ , and constant terms  $C_1 \sim C_{15}$  simulated by the virtual prototype in Table III. The constant terms of the evaluation parameters can be determined using quadratic interpolation fitting. The optimal target vibration transition time for  $t_s$ ,  $a_w$ , and  $P_{\max}$  is calculated based on the weighted root mean square value of acceleration and the maximum normal average pressure on the human-machine contact surface. The evaluation function for this target is derived from the results of the motion pair and spring probe in finite element simulation. The minimum value optimization objective  $F_{\min}$  of the comprehensive comfort evaluation index is established as the optimal solution of the multi-objective comfort optimization evaluation function.

By utilizing the finite element method [35], the vibration parameters can be optimized and adjusted to determine the damping coefficient  $C$  of the damper. The stiffness  $k$  of the torsion spring is subject to the constraint condition outlined in equation:

$$\begin{aligned} 0.05\text{N} \cdot \text{s} \cdot \text{mm}^{-1} &\leq C \leq 0.55\text{N} \cdot \text{s} \cdot \text{mm}^{-1} \\ 0.4\text{N} \cdot \text{m}^\circ &\leq k \leq 5.5\text{N} \cdot \text{m}^\circ \end{aligned} \quad (8)$$

Utilizing equations (3) ~ (6), a numerical simulation of population evolution is executed in equation (7). Upon reaching the convergence threshold, the optimal individual is selected, and its model is reconstructed for further finite element analysis of the virtual prototype.

#### 4. Co-simulation

The dynamic characteristics of exoskeleton wearable systems are too complex to be fully described by a single platform model alone. By utilizing both ANSYS and MATLAB platforms for co-simulation, a more accurate evaluation of system performance, mechanical response, dynamics performance, and stability indicators can be achieved. The comprehensive use of multiple platforms allows for a thorough assessment of exoskeleton wearable systems, providing a reliable basis for optimization and improvement.

##### 4.1. Virtual prototype simulation

In this study, the impact of the vibration parameters  $x_c$  and  $x_k$  on the comprehensive comfort index is explored, using them as independent variables. After selecting each set of parameters for the

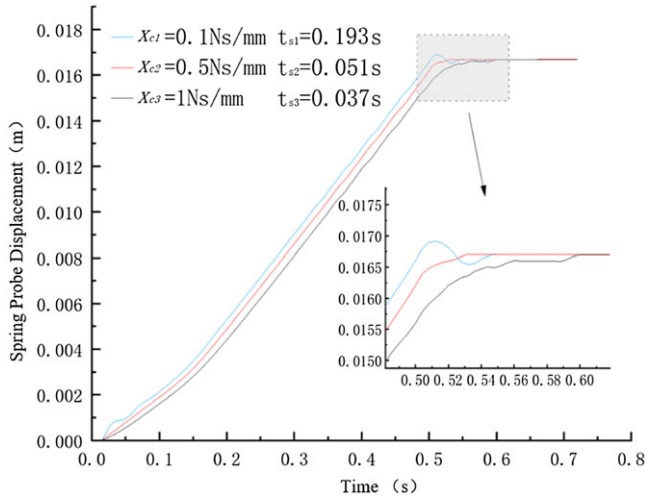


Figure 8. Changes in spring displacement in time domain.

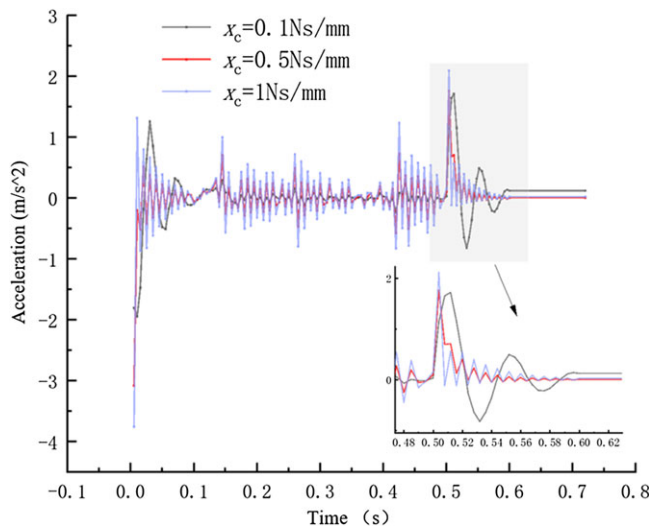


Figure 9. Changes in the time domain of spring acceleration.

human-machine parallel relaxation wearable system, ANSYS software is used to obtain optimized data results in the time domain for the stance phase (gait period: 0 ~ 0.72 s) [17].

The comfort of wearing an external skeleton is greatly influenced by the time interval  $t_s$  ( $t_s = 4T$ ,  $T$  is the characteristic parameter of the vibration) required for the spring probe displacement to restore balance. To optimize  $t_s$  for different vibration damping parameters  $x_c$ , the comfort evaluation function equation (3) is used. Additionally, equation (4) is utilized to extract the acceleration data in the time domain for accurate calculation of the weighted root mean square value of acceleration in the frequency domain. This data is then analyzed in Figs. 8 and 9.

After conducting a thorough analysis of Figs. 8, 9, and Table IV, it is evident that an increase in torsional stiffness and damping results in the following trends: ① The vibration transition time  $t_s$  is directly proportional to the overshoot, with a shorter transition time  $t_s$  leading to a smaller overshoot and improved wearing comfort; ② Both the weighted root mean square value of normal acceleration  $a_w$  and the pressure  $P_{max}$  at the wearing area will increase, which can negatively impact the comfort of wearing.

**Table IV.** Change results of wearing comprehensive comfort index under virtual prototype simulation.

<b>(a) Comfort metrics with variable damping parameters</b>			
<b>Damper Damping <math>C</math> (Ns/mm)</b>	$t_s$ (s)	$a_n$ (m/s <sup>2</sup> )	$P_{max}$ (Pa)
0.1	0.184	0.196	16 629.16
0.3	0.056	0.159	16 767.96
0.5	0.048	0.126	16 940.62
<b>(b) Comfort index under variable torsional spring stiffness parameters</b>			
<b>Torsion spring stiffness <math>k</math> (Nm/°)</b>	$t_s$ (s)	$a_n$ (m/s <sup>2</sup> )	$P_{max}$ (Pa)
0.5	0.152	0.304 6	17 411.19
1	0.128	0.305 6	17 425.41
5	0.056	0.334 6	17 981.98

### 4.2. Numerical optimization simulation

Based on the statistical data in Table IV and equations (3) ~ (5), evaluation models can be derived for the system’s vibration transition time  $t_s$ , the weighted root mean square value  $a_w$  of the normal acceleration at the knee joint’s exoskeleton-wearing point, and the maximum normal average pressure  $P_{max}$  of the human-machine contact surface. The vibration transition time  $t_s$  evaluation model is depicted in equation:

$$t_s(x) = 1.5x_c^2 - 1.24x_c + 0.0564x_k^2 - 0.341x_k + 0.694 \tag{9}$$

The evaluation model  $a_w$  of normal acceleration is depicted in equation:

$$a_w(x) = 0.055x_c^2 - 0.207x_c + 0.0019x_k^2 - 0.0045x_k - 0.1556 \tag{10}$$

The evaluation model of the  $P_{max}$  can be seen in equation:

$$P_{max}(x) = 0.0625x_c^2 + 0.0775x_c - 0.0004x_k^2 + 0.0104x_k - 0.1442 \tag{11}$$

The weight coefficients for the weighted root mean square value of normal acceleration, vibration transition time, and maximum average pressure in the lower limb exoskeleton human-machine parallel relaxation wearable system are determined to be 0.33 each. Consequently, a multi-objective evaluation model for the performance and optimization variables of the system is constructed based on equations (9) ~ (11), as shown in equation:

$$\min F(x) = 0.539x_c^2 - 0.4565x_c + 0.4565x_k^2 - 0.4565x_k + 0.1314 \tag{12}$$

The establishment of a multi-objective evaluation function using MATLAB software programming is described in equation 10. The initial population for optimization consists of the structural and material parameters of the tension and relaxation wearable system. Surface graph can be generated to visualize the optimization process, as shown in Figure 10. Using a multi-objective genetic algorithm [36] with a population size of 200, 100 elites, and a cross-offspring ratio of 0.6, parameters such as maximum effective stress, maximum effective deformation, and the proportion of effective stress nodes can be optimized. After multiple generations of optimization, the final optimal individual is determined to be  $(C, k) = (0.302, 1.098)$ .

### 4.3. Integrated validation

To validate the efficiency of the equivalent nonlinear contact stiffness model, the optimal individual is reconstructed, and the overall dynamics analysis of the human-machine parallel system is conducted. Figs. 11 and 12 display the stress and deformation cloud maps of the system under assisted working conditions. Figure 13 compares the optimization results of the acceleration amplitude of the lower limbs in the stance phase in the frequency domain.

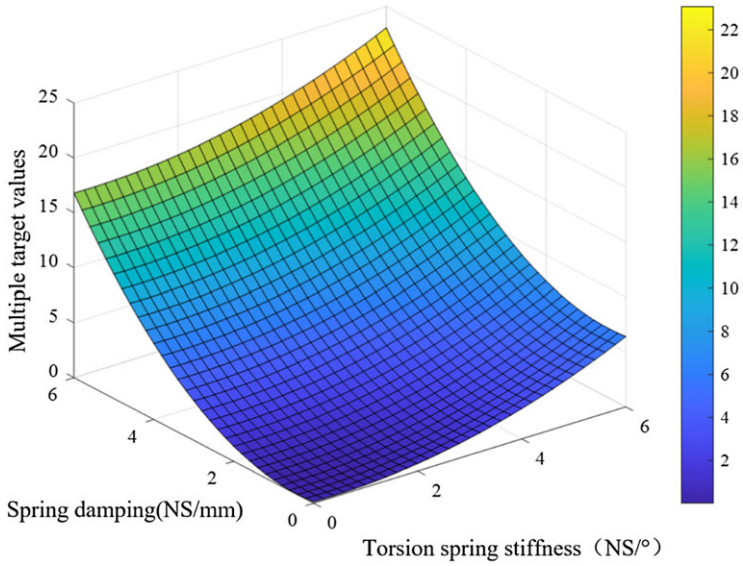


Figure 10. Multi-objective evaluation model.

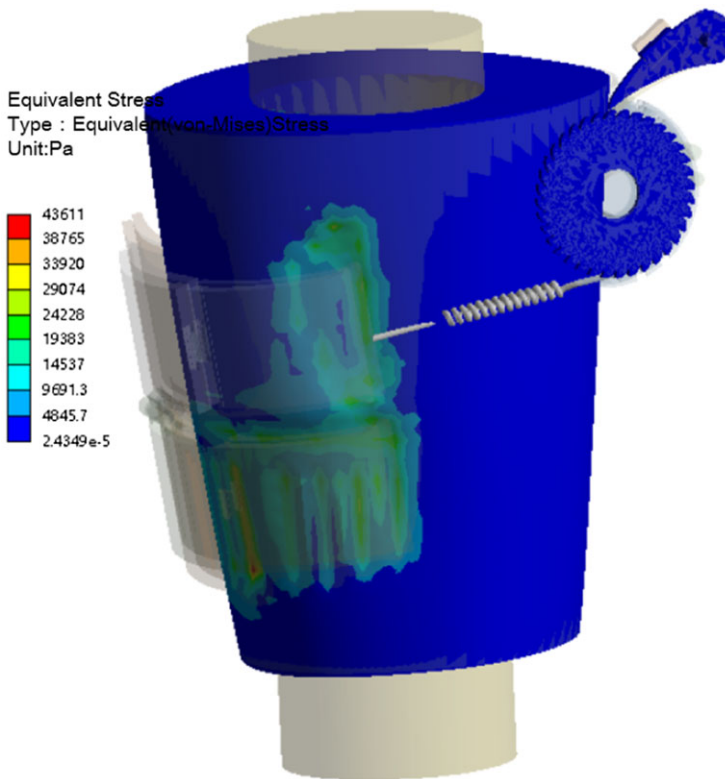


Figure 11. Stress nephogram of human exoskeleton system.

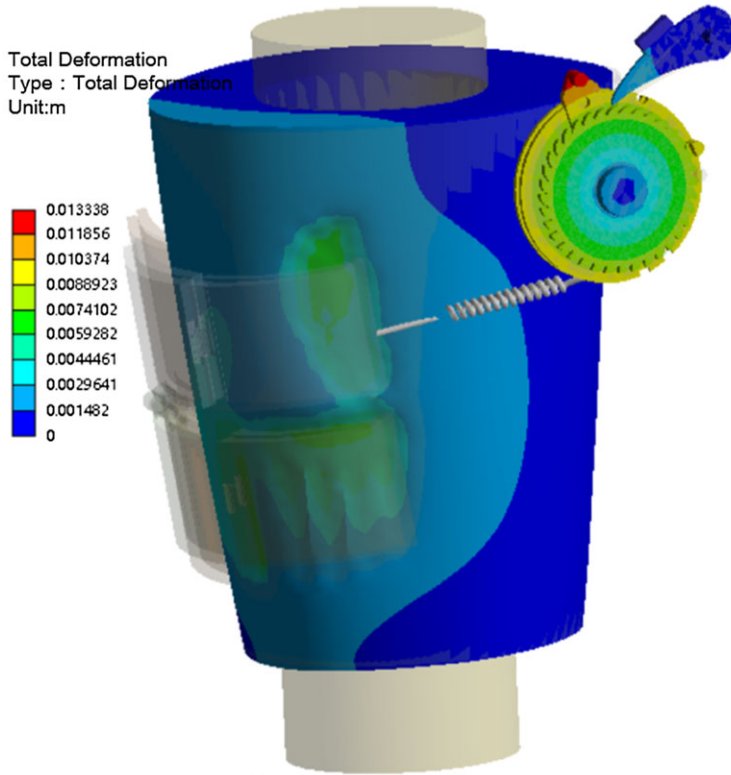


Figure 12. Deformation nephogram of human exoskeleton system.

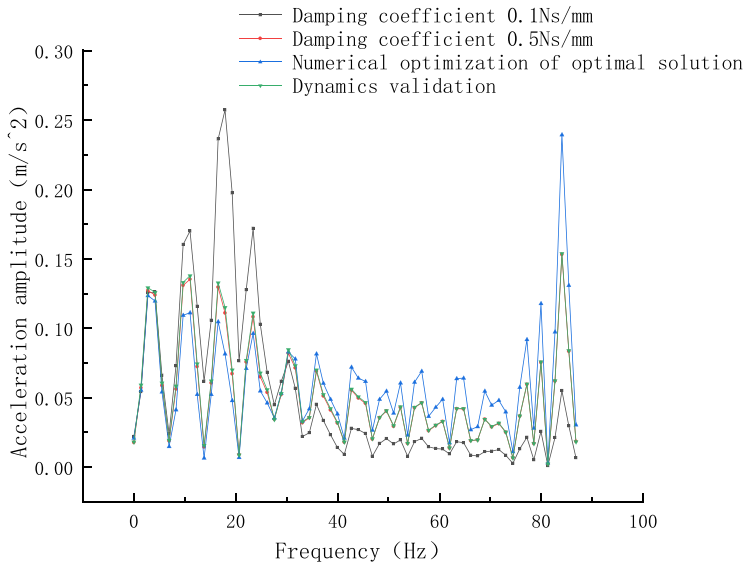


Figure 13. Change of acceleration in frequency domain before and after optimization.

After conducting data comparison and analysis, it is found that the stress and deformation observed in Figs. 11 and 12 align with the maximum effective stress and deformation experienced while wearing the lower limb exoskeleton as described in reference [19]. Additionally, the weighted acceleration values correspond to the acceleration curve of the human-machine parallel vibration model that is separately simulated. It is also determined that the optimized exoskeleton meets the comfort requirements outlined in Table II, specifically ensuring that the root mean square value of the normal acceleration borne by the human body is less than  $0.315 \text{ m/s}^2$ . As a result, the effectiveness of the equivalent model has been successfully demonstrated.

The comparison of all multi-objective values before and after optimization is presented in Table III. Upon analyzing the data, it is observed that sacrificing less than 1% of the pressure value at the wearing area led to a 69% increase in vibration transition time  $t_s$  and an 18% increase in the weighted root mean square value  $a_w$  of normal acceleration. Overall, the optimization significantly enhanced the wearing comfort of the knee joint exoskeleton human-machine parallel relaxation wearable system.

## 5. Conclusion and discussion

This paper introduces a research prototype of a wearable knee exoskeleton system that incorporates an overrunning clutch for tension and relaxation control. The study extensively investigates the system's operational principles, analyzing nonlinear trajectory data collected from the exoskeleton attachment points through the concept of functional equivalence. Furthermore, a nonlinear contact stiffness model is developed from this data to assess the system's rigid-flexible coupling dynamics.

A new evaluation index for wearable comfort is proposed, which takes into account the vibration transition time  $t_s$ , the weighted root mean square value  $a_w$ , and the maximum normal average pressure  $P_{\max}$ . This index is based on the analysis results of the equivalent model. The optimization problem for this evaluation index is reduced to a two-parameter optimization problem for the design variables  $C$  and  $k$  of the exoskeleton wearable system.

A co-simulation is conducted by integrating a multi-objective genetic algorithm with finite element analysis to optimize the wear parameters of the buffer layer. This optimization leads to a 19% decrease in the vibration transition time  $t_s$  and a 69% reduction in the weighted root mean square value  $a_w$  of the normal acceleration at the wearing area, ultimately improving the wearing comfort of the exoskeleton.

**Author contribution.** Yuwei Yang, Jiapeng Yin, and Jinyou Xu have significantly contributed to data collection, data analysis, and paper writing. Wenyao Qi, Zhaotong Li, and Zuyi Zhou have made significant contributions to experimental design and paper writing. Zhongyu Liu has significantly contributed to the data collection process.

**Financial support.** This work was supported by the National Natural Science Foundation of China (Grant no. 10101/70305901).

**Competing interests.** The authors declare no conflicts of interest exist.

**Ethical approval.** None.

## References

- [1] S. Wu, X. Zhang and Y. Chen, "Quality of life of patients with osteoarthritis of the knee joint and factors affecting it," *Qilu Nurs J* **22**(2), 56–58 (2016).
- [2] J. Jahn, Q. T. Ehlen and C. Y. Huang, "Finding the goldilocks zone of mechanical loading: A comprehensive review of mechanical loading in the prevention and treatment of knee osteoarthritis," *Bioengineering* **11**(2), 110 (2024).
- [3] R. Seil and D. Pape, "Causes of failure and etiology of painful primary total knee arthroplasty," *Knee Surg Sports Traumatol Arthrosc* **19**(9), 1418–1432 (2011).



- [4] J. Wei, S. Zhang and J. Zhang, "Biofusion design and parameter optimization for a novel passive assisted knee exoskeleton robot based on eight-bar mechanism," *Robotica* **42**(6), 1959–1985 (2024).
- [5] J. Wang, X. Li, T.-H. Huang, S. Yu, Y. Li, T. Chen, A. Carriero, M. Oh-Park and H. Su, "Comfort-centered design of a lightweight and backdrivable knee exoskeleton," *IEEE Robot Autom Lett* **3**(4), 4265–4272 (2018).
- [6] Y. Long and Y. Peng, "Design and control of a quasi-direct drive actuated knee exoskeleton," *J Bionic Eng* **19**(3), 678–687 (2022).
- [7] B. Ostrach and R. Riemer, "Simulation of a passive knee exoskeleton for vertical jump using optimal control," *IEEE Trans Neur Syst Rehabil Eng* **28**(12), 2859–2868 (2020).
- [8] H. Li, D. Sui, H. Ju, Y. An, J. Zhao and Y. Zhu, "Mechanical compliance and dynamic load isolation design of lower limb exoskeleton for locomotion assistance," *IEEE/ASME Trans Mechatron* **27**(6), 5392–5402 (2022).
- [9] Y. Zimmermann, J. Song, C. Deguelle, J. Läderach, L. Zhou, M. Hutter, R. Riener and P. Wolf, "Human-robot attachment system for exoskeletons: Design and performance analysis," *IEEE Trans Robot* **39**(4), 3087–3105 (2023).
- [10] W. Yang, Z. Yan, L. Yu, L. Xu, X. Liu and C. Yang, "Phase oscillator optimization eliminates jittering during transition gaits in multimodal locomotion assisted by a portable hip exoskeleton," *Robotica* **41**(11), 3349–3360 (2023).
- [11] X. Yang, G. Zhao and Y. Liang, *Control Theory and Technology of Lower Limb Intelligent Carrying Exoskeleton System* (National Defense Industry Press, Beijing, 2017) pp. 17–20.
- [12] S. Y. Gong, "MATLAB-based oscillatory phase simulation of lower limb prostheses," *J Hebei Univ Technol* **40**(2), 6–9 (2011).
- [13] J. Sun, F. Hu, K. Gao, F. Gao, C. Ma and J. Wang, "Research and experiment on active training of lower limb based on five-bar mechanism of man-machine integration system," *Robotica* **42**(5), 1453–1475 (2024).
- [14] L. Zhou, W. Chen, J. Wang, S. Bai, H. Yu and Y. Zhang, "A novel precision measuring parallel mechanism for the closed-loop control of a biologically inspired lower limb exoskeleton," *IEEE/ASME Trans Mechatron* **23**(6), 2693–2703 (2018).
- [15] D. B. Fineberg, P. Asselin, N. Y. Harel, I. Agranova-Breyter, S. D. Kornfeld, W. A. Bauman and A. M. Spungen, "Vertical ground reaction force-based analysis of powered exoskeleton-assisted walking in persons with motor-complete paraplegia," *J Spinal Cord Med* **36**(4), 313–321 (2013).
- [16] L. P. Jose, *Wearable Robots: Biomechatronic Exoskeletons* (John Wiley & Sons, Ltd, West Sussex, 2008) pp. 23–27.
- [17] T. A. Krouskop, R. Williams, M. Krebs, I. Herszkowicz and S. Garber, "Effectiveness of mattress overlays in reducing interface pressures during recumbency," *J Rehabil Res Develop* **22**(3), 7–10 (1985).
- [18] Y. Luan, J. Zhang and K. Qi, "Comfort optimization of a novel foot mechanism for lower limb exoskeleton," *J Biomed Eng* **37**(02), 324–333 (2020).
- [19] B. Liu, Y. Liu, Z. Zhou and L. Xie, "Control of flexible knee joint exoskeleton robot based on dynamics model," *Robotica* **40**(9), 2996–3012 (2022).
- [20] B. Chen, B. Zi, L. Qin and Q. Pan, "State-of-the-art research in robotic hip exoskeletons: A general review," *J Orthop Translat* **20**, 4–13 (2020).
- [21] Z. Xu, F. Yu and Z. Zhang, "Joint simulation of vehicle cornering brake ABS based on ADAMS and simulink," *China Mech Eng* **20**(07), 877–881 (2009).
- [22] V. Lajeunesse, C. Vincent, F. Routhier, E. Careau and F. Michaud, "Exoskeletons' design and usefulness evidence according to a systematic review of lower limb exoskeletons used for functional mobility by people with spinal cord injury," *Disabil Rehabil: Assist Technol* **11**(7), 535–547 (2016).
- [23] Y. Yang, H. Zhao and B. Li, "An adaptive variable stiffness extracorporeal knee joint device with intelligent tensioning function," *China* **20210026090**, 1–12 (2020).
- [24] Y. Yang, W. Ge and Z. Liu, "In vitro flexible knee joint," *China* **201510929833**, 1–8 (2015).
- [25] C. Tudor-Locke, W. D. Johnson and P. T. Katzmarzyk, "Accelerometer-determined steps per day in US adults," *Med Sci in Sports Exerc* **41**(7), 1384–1391 (2009).
- [26] J. Shen, S. Zhang, C. Chen and Z. Xu, "Research progress of unpowered exoskeleton assist robot," *J Mech Transm* **44**(2), 166–176 (2020).
- [27] S. El Hraiech, A. H. Chebbi, Z. Affi and L. Romdhane, "Genetic algorithm coupled with the Krawczyk method for multi-objective design parameters optimization of the 3-UPU manipulator," *Robotica* **38**(6), 1138–1154 (2020).
- [28] Y. Choi, Y. Kim, M. Kim and B. C. Yoon, "Muscle synergies for turning during human walking," *J Mot Behav* **51**(1), 1–9 (2019).
- [29] L. Fu and J. Zhao, "Maxwell-model-based compliance control for human-robot friendly interaction," *IEEE Trans Cogn Develop Syst* **13**(1), 118–131 (2021).
- [30] L. Zhang, L. Shen and M. Zhu, "Nonlinear finite element analysis of gait processes in thigh residual limbs," *Med Biomech* **28**(04), 397–402 (2013).
- [31] J. Hu, L. Liang and B. Zeng, "Design, modeling, and testing of a soft actuator with variable stiffness using granular jamming," *Robotica* **40**(7), 2468–2484 (2022).
- [32] K. Iida and K. Ono, "Design consideration of contact/near-contact sliders based on a rough surface contact model," *J Trib* **125**(3), 562–570 (2003).
- [33] L. Zhao and J. Fan, "Multi-objective optimization design of coal mining machine spiral drum based on genetic algorithm," *China Mech Eng* **29**(05), 591–596 (2018).
- [34] General Administration of Quality Supervision, Inspection and Quarantine of the People's Republic of China, *Mechanical Vibration and Shock - Evaluation of Human Exposure to Whole-Body Vibration*, **GB/T13441** (China Standard Press, Beijing, 2007). 2007/ISO22631-1: 1997).

- [35] S. E. Randall, D. M. Halsted III and D. L. Taylor, "Optimum vibration absorbers for linear damped systems," *J Mech Des* **103**(4), 908–913 (1981).
- [36] A. Rosyid, B. El-Khasawneh and A. Alazzam, "Genetic and hybrid algorithms for optimization of non-singular 3PRR planar parallel kinematics mechanism for machining application," *Robotica* **36**(6), 839–864 (2018).

---

**Cite this article:** Y. Yang, J. Yin, W. Qi, Z. Li, Z. Zhou, Z. Liu and J. Xu (2024). "Optimization and synthesis on the dynamics performance of the tensioning and relaxing wearable system in a novel knee exoskeleton using co-simulation", *Robotica* **42**, 3918–3933. <https://doi.org/10.1017/S0263574724001723>